RSC Advances

ROYAL SOCIETY OF CHEMISTRY

www.rsc.org/advances

Single and Bicomponent Anionic Dyes Adsorption Equilibrium Studies on Magnolia-Leaf-Based Porous Carbons

Huijing Yu,[a] Tingting Wang,[a] Wei Dai,*[a] Xianxing Li,[a] Xin Hu,[a] and Na Ma*[b]

[a]College of Chemistry and Life Science, Zhejiang Normal University, Zhejiang Province Jinhua 321004, People's Republic of China

[b]College of Geography and Environmental Sciences, Zhejiang Normal University, Zhejiang Province Jinhua 321004, People's Republic of China

ABSTRACT: A new type of porous carbon are prepared by cost-effective pyrolysis carbonization and the subsequent alkali activation of an easily available biomass, magnolia leaf (ML). The as-prepared ML porous carbons (MPCs) show high specific surface areas, suitable pore size distributions. Surface characterization of ML and MCP-1 were investigated by N_2 adsorption, FT-IR, SEM and TEM. Two anionic azo dyes were used, namely orange II (OII) and methyl orange (MO) to simulate the textile effluent. Batch experiments of OII and MO in single dye system (SDS) and binary dye system (BDS) onto MCP-1 were investigated as a function of pH, contact time and species concentrations. The adsorption process followed the Langmuir isotherm model with high coefficients of correlation (R^2> 0.999). The pseudo second order kinetic model fitted well in correlation to the experimental results. This work indicates that MPCs demonstrated a superior OII and MO adsorption capabilities and could be employed as a low cost alternative to commercially available porous carbon in the removal of dyes from wastewater.

Keywords: Adsorption; Magnolia leaf; Porous carbons; Waste-water treatment;

Anionic Azo dyes

1. Introduction

Dyes discharged together with industrial textile wastewaters are main organic pollutants because they are highly visible and undesirable even at low concentrations in water.[1] Discharging of dye-containing effluents into hydrosphere is prohibited not only because of their color, which reduces the sunlight penetration into the water, but also because of toxic, carcinogenic and mutagenic nature of their breakdown products.[2,3] Among different types of dyes, OII and MO are well-known typical acidic/anionic and azo dyes, and have been widely used in textile, printing, paper, food and pharmaceutical industries and research laboratories.[3] The structures of OII and MO are similar and shown in Scheme 1. As known from Scheme 1, due to one more benzene ring in the structure, the molecular weight and size of OII are relative larger than MO as the typical representative azo dyes. Acute exposure to OII and MO can cause increased heart rate, vomiting, shock, cyanosis, jaundice, quadriplegia, and tissue necrosis in humans.[4] Thus, simultaneously removal of OII and MO from wastewater and/or process effluent is very important due to their potential toxicity to human and environment. OII and MO for the reasons stated above were selected in this work as the model dye textile effluent.

Various methods such as chemical precipitation,[5,6] ion exchange,[7,8] membrane filtration,[9,10] physical adsorption,[11,12] chemical oxidation/reduction,[13,14] and bioremoval[15,16] have been developed in the removal of dyes from wastewater. Among these, the adsorption technique is considered as a competitive method for treatment of

dyestuff wastewater due to its easy handling, high efficiency, and economic feasibility.[17] The adsorbents with high capacity and high rate play a critical role in the adsorption removal of dye molecules. The porous carbon material (PCM) is a commercial adsorbent for eliminating pollutions from wastewater and air. However, the higher production cost, and regeneration difficulty of PCM limit its widespread use.[18,19] Currently, there are many studies on the development of low-cost adsorbents, namely by using waste materials for that purpose.[20] PCM can be generally acquired by simple carbonization and activation treatment of cheap and easily available natural biomass wastes or carbonaceous minerals using different porogens.[20,21] Hence, the preparation of PCM from natural feedstock has received extensive concerns. All kinds of raw materials including sugar cane bagasse,[22] tea-leaves,[23] pulps, peels or seeds of fruits,[24-26] sunflower seed shell,[27] porous starch,[28] even pitch[29,30] were widely employed as precursors to afford porous carbons as adsorbents for the removal of specific pollutants from aqueous phase.

Magnolia, a type of deciduous tree, is widely grown in most regions of China for the robust cold and drought tolerance. As a rather low, rounded, thickly branched, and coarse-textured tree, the height of magnolia tree can hit to 30 feet (9.1 m). The magnolia leaves (MLs) are ovate, bright green, 15 cm long and 8 cm wide, which endow MLs with good antiviral and antibacterial efficacies.[31] Nevertheless, in most cases, MLs were discarded and rotted away into soil without effective utilizations. Given the porous texture and the containing of various organic compounds, ML is an optional precursor for preparing of porous carbon material (Magnolia-leaf-based

porous carbons, MPCs) and the dyes adsorption performance is also expectable.

In this study, we synthesized a novel three-dimensional magnolia-leaf-based porous carbon by high temperature carbonization and alkali activation. Two similar structure organic dyes (OII and MO) were used as model pollutants to investigate the adsorption characteristics of as-prepared adsorbent in SDS and BDS systems. The remarkably enhanced specific surface areas, versatile pore texture with the coexistence of micro-pores and meso-pores structure, apparently increased hydrophilicity and moderate graphitization made the as-prepared MCPs high adsorption performance to remove OII and MO from aqueous solution. The influence of several operating parameters such as dye concentration, contact time, adsorbent dosage, pH and temperature was investigated. Equilibrium isotherms and kinetics modelling were used to investigate the possible mechanism of the adsorption process.

2. Experimental section

2.1. Materials

Potassium hydroxide (KOH), hydrochloric acid (HCl) and sodium hydroxide (NaOH) used in this work were purchased from the Sinopharm Chemical Reagent Co., Ltd, China. They were both of analytical grade and were used as received without further purification. An aqueous stock solution of OII and MO was prepared by dissolving the OII ($C_{16}H_{11}N_2NaO_4S$, MW: 350.32, Sigma-Aldrich) and MO ($C_{14}H_{14}N_3NaO_3S$, MW: 327.34, Sigma-Aldrich) in deionized water. One type of commercial active carbon, coconut shell-based activated carbon, CS-AC was obtained from Chemical Reagent Co., Ltd, China. The BET surface area and total volume of

CS-AC is 1202 m^2/g and 1.07 cm^3/g, respectively. Deionized water was used to prepare the desired concentrations of model dye waste water.

2.2. Preparation of MPCs

The MPCs was prepared by a similar KOH activation procedure that was previously proposed by our group.[2,19] In a typical preparation, 2 g of precursor (MLs) in the particle size 150 μm was mixed with 8 g of KOH powder. Hence, the mass ratio of KOH and MLs precursor was 4:1 and the resulting mixture was placed into a horizontal pipe reactor (50 mm o.d.) for activating as follows. (i) Nitrogen gas was allowed to flow through the reactor at a rate of 40 mL/min and maintained at this flow rate throughout the whole activation process. (ii) The temperature of the reactor was raised to the activation temperature (1073 K) at a heating rate of 1 K/min. (iii) The reactor was held at the activation temperature for 40 min. (iv) Finally, it was cooled down to room temperature. The samples thus obtained were washed with distilled water until the filtrate appeared neutral. The final samples (MPC-1) were obtained by heating these samples at 423 K under vacuum for 24 h.

2.3. Porous carbon characterization

Specific surface areas and pore volumes were determined by N_2 adsorption. An automated adsorption apparatus (Micromeritics, ASAP 2020) was used for the measurements. N_2 adsorption was carried out at liquid N_2 temperature (77 K). The specific surface areas were calculated using the BET equation by assuming a section area of nitrogen molecule to be 0.162 nm^2. The *t*-plot method was applied to calculate the micro-pore volumes and surface areas. The total pore volume was estimated to be

the liquid N_2 volume at a relative pressure of 0.99. The pore size distribution was calculated by density functional theory (DFT). The morphologies of prepared MPCs and raw material (MLs) were examined by scanning electron microscopy (SEM) (300 K Pixel CMOS). FT-IR spectra for the samples were recorded on a Nexys 670 FT-IR spectrometer (Nicolet Instrument Co., USA). The transmission spectra of the samples were recorded using KBr wafers containing 0.5 wt % of samples. These wafers were dried over night at 393 K before the spectra were recorded. The spectra were obtained by scans of 64 scans with a resolution of 4 cm^{-1}.

2.4. Batch equilibrium studies

The equilibrium isotherms of OII and MO adsorption on MPC-1 were determined by performing adsorption tests in 100 mL erlenmeyer flasks where 50 mL of OII and MO solutions with different initial concentrations (100-1000 mg/L) were placed in each flask. To determine the adsorption capacities at various pHs, the pH of the dye solutions was adjusted with 0.1M HCl or 0.1M NaOH aqueous solution. 0.02 g of each of the prepared MPC-1, with particle size of 110 μm, were added to each flask and kept in a shaker with 150 rpm at room temperature (298 K) for 3 h to reach equilibrium. Then the samples were filtered and the residual concentrations of OII and MO in the filtrate were analyzed by a UV-Visible spectrophotometer (Thermo Fisher Evolution 300 PC) at maximum wave lengths of 485 and 464 nm, respectively. It was found that the calibration curves were very reproducible and linear over the concentration range used in this work. The adsorbed amount of OII and MO at equilibrium, q_e (mg/g) was calculated by the following expression:

$$q_e = \frac{(C_o - C_e)\cdot V}{W} \qquad (1)$$

where C_o and C_e (mg/L) are the initial and equilibrium concentrations of OII and MO solution, respectively; V (L) is the volume of solution, and W (g) is the weight of MCP-1 used. Duplicate experiments were carried out for all the operating variables studied and only the average values were taken into consideration. The average deviation of duplicate results in the units of concentration was found to vary between ±1%.

The batch experiments of binary dye solution were performed with a similar procedure. In a binary system with components A (OII) and B (MO), the measurement would be carried out at their maximum absorbance wavelength λ_{max1} and λ_{max2}, respectively, giving absorbances of A_1 and A_2. Concentrations of dye solution were then estimated quantitatively using the linear regression equations obtained by plotting a calibration curve for each dye over a wide range of concentrations. In a binary dye solution, the concentrations of OII and MO were calculated according to the literature.[32] In a binary system with components A and B, dye concentrations were calculated by the following equations:[32]

$$C_A = \frac{k_{B_2}A_1 - k_{B_1}A_2}{k_{A_1}k_{B_2} - k_{A_2}k_{B_1}} \qquad (2)$$

$$C_B = \frac{k_{A_1}A_2 - k_{A_2}A_1}{k_{A_1}k_{B_2} - k_{A_2}k_{B_1}} \qquad (3)$$

where k_{A1}, k_{B1}, k_{A2}, and k_{B2} are the calibration constants for components A and B at wavelengths λ_{max1} and λ_{max2}, respectively giving absorbances of A_1 and A_2. k_{A1}, k_{B1}, k_{A2}, and k_{B2} for components A and B were obtained using the linear regression equations

according to the calibration curve. For binary dye solutions, initial dye concentrations were maintained at 1:1 (w/w).

3. Results and discussion

3.1 Material characterization

The nitrogen adsorption isotherm graph of MPC-1 at 77 K is shown in Fig. 1. The isotherm displays type I shape according to the IUPAC classification.[17,19] The pore size distribution calculated by density functional theory (DFT) proved that the pore size of MPC-1 mainly focused on 2 nm. The specific BET surface area and pore volume of MPC-1 sample were 2834 m^2/g and 1.58 cm^3/g, respectively. The huge surface area of the MPC-1 could provide the huge capacity for dye molecules' adsorption inside the pore structure. The SEM micrographs of ML and MPC-1 were presented in Fig.2 to analyze its surface shape. Based on the analysis of the images taken by SEM before and after the KOH chemical activations process, two distinct types of shapes were observed. The surface of ML (Fig. 2(A)) was fairly smooth, with few cracks or voids. While the SEM micrograph (Fig. 2(B)) of MPC-1 particles showed cavities, pores and more rough surfaces due to the carbonization and KOH activation process. The surface area of the MPC-1 will be enhanced by the presence of more porosity, which can hold more dye molecules from solution during adsorption. This means that the KOH activation has an influence on pore development during the preparation process. This phenomenon of the activation process is found similar to a previous study.[2,19] FT-IR transmission spectra (Fig. 3) were obtained to characterize the surface groups of ML and MPC-1 samples. As known in Fig. 3, the FTIR

spectroscopic analyses of MPC-1 and ML indicated broad bands at 3440 cm^{-1} representing bonded –OH groups. The band at 2930 cm^{-1} indicates the presence of an aliphatic –CH stretching. The band at 2358 cm^{-1} is the C≡C stretching vibrations in alkyne groups. The band at 1728 cm^{-1} denotes the existence of carbonyl/carboxyl groups. The 1610 cm^{-1} band indicates the presence of an aromatic C=C ring stretching. The bands observed at 1388 cm^{-1} could be assigned to symmetric bending of C–H. The band at 1068 cm^{-1} indicates the C–O stretching vibrations in alcohols, phenols or ether or ester groups. The peak observed at 400–700 cm^{-1} could be due to C–C stretching. After KOH activation process, many groups of ML are destroyed and possessed aromatic structure and oxygen groups. Thus, the FTIR analysis indicates that the MPC-1 is represented by functional groups such as O-H, COOH, CO, C-C, C≡C and C=C that could be potential adsorption sites for interaction with the anionic dyes. Such finding is similar to that made in the literatures.[33,34]

3.2. Effect of adsorbent dosage and pH

The dependence of adsorption of the OII and MO on the concentration of model waste water in SDS and BDS systems were investigated by varying the quantity of the MPC-1 adsorbent from 0.005 to 0.05 g in 50 mL of 1000 mg/L solution of the dye while keeping other parameters (contact time 3 h, agitation speed 150 rpm, particle size 110 μm, 298 K) constant. As shown in Fig. 4, the adsorption capacities of OII and MO in the first stage increase rapidly with the increase in the adsorbent dose, and then the adsorption capacities are not changed significantly with the further increase in the adsorbent dose. It can be seen that the adsorption capacities of the dyes reach

saturation with the adsorbent dose more than 0.4 g/L. Thus, 0.4 g/L was chosen as the optimum dose and used in the further experiments. The two-stage-dependent adsorption behavior was also agreement with the literatures.[19,35] This observation is usually attributed to the increase in the adsorbent pore surface areas and availability of more adsorption sites with increasing mass of adsorbent.

The effect of the solution pH on the adsorption of dyes on MPC-1 in SDS and BDS systems is shown in Fig. 5. For both OII and MO, the adsorption capacities at low pH were larger than those at high pH in both SDS and BDS systems. In addition, the effects of solution pH for OII and MO adsorption were different. When the solution pH was varied from 2 to 10, the OII and MO uptake capacities in SDS decreased from 1920 and 1419 mg/g to 1488 and 869 mg/g (decreased 26 % and 39 %, respectively); However, the their capacities in BDS decreased from 1094 and 616 mg/g to 951 and 447 mg/g (decreased 13 % and 27 %, respectively). This discrepancy suggests the presence of competitive adsorption for OII and MO adsorption onto MPC-1 in BDS.

The mechanism of dyes adsorption onto porous carbons is controlled by various factors like physical and/or chemical properties of porous carbons, molecular structure of dyes, hydrophobie bonds, electrostatic force, mass transfer process, van der waals force and hydrogen bond formation, etc.[17,19,35] As known in Scheme 1, OII and MO are ideally planar molecule and therefore can easily adsorb on MPC-1 by π-π stacking interaction between the aromatic backbone of the dye and hexagonal skeleton of MPC-1. Thus, we think that the larger uptake capacity of OII than MO comes from the OII structure having a stronger π-π stacking interaction with MPC-1

due to its expanded aromatic ring. Such finding is similar to that made in previous works.[17,19] Usually, there are oxygen-containing groups at surface of the porous carbon (COOH, C-OH, etc). Thus, the surface charge of the porous carbon is dependent on the solution pH. At high solution pH, the porous carbon became negatively charged and the anionic dyes investigated in this work should experience an electrostatic repulsion force upon adsorbing onto the surface of the porous carbon. However, at the appropriate low pH solution, the porous carbon is electrically neutral and thus favors the dye adsorption, as observed in Fig. 5 with a higher adsorption capacity for OII and MO at acidic solution. Therefore, we think that both the electrostatic force and π-π stacking interactions are contributive to the dye adsorption.

3.3. Adsorption isotherms

The experimental data at equilibrium between the amount of adsorbed dye (in SDS and BDS) (q_e) on the adsorbent (MCP-1) and the concentration of dye solution (C_e) at a constant temperature and pH were used to describe the optimum isotherm model. The linear forms of Langmuir,[36] Freundlich,[37] Temkin[38] and D-R[39] isotherm models equations were used to describe the equilibrium data. Applicability of these equations was compared by judging with the correlation coefficients (R^2). In this work, adsorption isotherm experiments were carried out at initial dye concentrations of 100–1000 mg/L. Isotherm parameters, evaluated from the linear plots of equations (4–7) are illustrated in Table S.I.1. The value of q_m, K_L are presented in Table S.I.2. The q_m value for the Langmuir I isotherm in SDS system are 1488 (OII) and 869 (MO) mg/g, and 951 (OII) and 447 (MO) mg/g in BDS. The adsorption coefficients (K_L, related to

the apparent energy of sorption) were found to be 0.25 (OII) and 0.50 (MO) for SDS and 0.21 (OII) and 0.41 (MO) L/g for BDS. The R^2 (correlation coefficient) value of >0.999 indicated that the Langmuir isotherm is good for explaining the sorption of OII and MO on MPC-1 in two systems. The q_m indicates the efficiency of an adsorbent for an adsorbate was found to be lower in BDS than SDS, as a result of the competition between dyes molecular and the two azo dyes in the former.

To investigate the possible multilayer adsorption and non-linear energy distribution of the adsorption sites, the Freundlich isotherm was studied. The intercept value (K_f) and the slope n (Table S.I.2) were obtained from the linear plots of Freundlich isotherm (not shown) at room temperature (298 K). The values of R^2 for Freundlich plots were 0.9855 (OII) and 0.8789 (MO) for SDS and 0.9417 (OII) and 0.9178 (MO) for BDS. The values of 1/n were 0.07 (OII) and 0.05 (MO) for SDS and 0.12 (OII) and 0.03 (MO) for BDS. The values of 1/n (indicative of favorability) from Freundlich isotherm model, ranging from 0 to 1, is a measure of adsorption intensity or surface heterogeneity that becomes more heterogeneous as its value gets closer to zero. A value for 1/n below 1 indicates a normal Langmuir adsorption isotherm, while 1/n above 1 is indicative of cooperative adsorption.

Temkin adsorption was chosen to fit the equilibrium adsorption data. The parameters, K_T and b_T of the Temkin equation have been calculated for OII and MO adsorption in both systems (Table S.I.2). The Temkin adsorption potential (K_T) values were found to be 6.6×10^4 (OII) and 5.7×10^6 (MO) for SDS and 582 (OII) and 4.4×10^{11} (MO) L/g for BDS. The Temkin constant (b_T) values, related to heat of

sorption, were found to be 28 (OII) and 60 (MO) for SDS and 30 (OII) and 180 (MO) kJ/mol for BDS. However, the typical range of bonding energy for ion-exchange mechanism is 8–16 kJ/mol.[19] Since the range of bonding energy associated with the adsorbent under study were found to be substantially low, the interaction between dyes and MPC-1 in both systems seems not have involved ion–exchange mechanism, but rather physisorption mechanism.

The Dubinin-Radushkevich (D-R) model is often used to estimate the characteristic porosity and the apparent free energy of adsorption. The isotherm parameters from the linear plots of the isotherm (not shown) are given in Table S.I.2. Although the adsorbent showed relatively lower R^2 values (0.7117 (OII) and 0.9609 (MO) for SDS and 0.5366 (OII) and 0.9232 (MO) for BDS) compared to the preceding models (i.e., Langmuir, Freundlich and Temkin isotherms), yet it is significant enough for deriving information regarding the adsorption. The values of sorption affinity (q_s) of dyes for MCP-1, as per for D-R model are 1393 (SDS) and 827 mg/g (BDS). The calculated mean energy of adsorption, E, from the D-R isotherm, gives information about the chemical or physical properties of the sorption. The calculated mean energy value of adsorption of dyes by MCP-1 is low (5 kJ/mol) and this implies that the type of adsorption appears to be physical processes because chemisorption processes have adsorption energies greater than 20 kJ/mol.[19]

The equations of a competitive Langmuir model[28] are as follows:

$$q_{e1} = \frac{q_{\max 1} K_{L1} C_{e1}}{1 + K_{L1} C_{e1} + K_{L2} C_{e2}} \qquad (8)$$

$$q_{e2} = \frac{q_{\max 2} K_{L2} C_{e2}}{1 + K_{L1} C_{e1} + K_{L2} C_{e2}} \qquad (9)$$

where K_{L1} and K_{L2} are the Langmuir constants of the adsorbates 1 and 2, $q_{\max 1}$ and $q_{\max 2}$ are the maximum adsorption capacity of the adsorbates 1 and 2.

Adsorption isotherms of OII and MO on MPC-1 in SDS and BDS are shown in Fig. 6. The adsorption capacities of OII and MO onto MPC-1 were reduced from 1488 mg/g (SDS) to 951 mg/g (BDS) and from 869 mg/g (SDS) to 447 mg/g BDS), respectively, at pH 7 because of the highly contention on active sites between two types of dye molecules in the binary system. MO has a lower molecular weight than that of OII, the adsorption capacity of OII is higher than that of MO at pH 7. The experimental data in the binary systems were applied to the competitive Langmuir equations (Table S.I.3). The correlation coefficients in the binary system were lower than in single dye system. We can say that the adsorbent surface is homogeneous and there is no interaction between the adsorbed molecules. These systems are applied to real systems due to the effect of surface heterogeneity and interaction between azo dye molecules. The MO and OII adsorption performance of CS-AC and ML samples were investigated by the batch test (The same experiment condition can be found in section 2.4). As a result, the OII uptake capacities of CS-AC and ML are 322 and 128 mg/g in SDS, 286 and 79 mg/g in BDS. The MO uptake capacities of CS-AC and ML are 315 and 115 mg/g in SDS, 280 and 72 mg/g in BDS. The adsorption capacities of OII and MO on CS-AC and ML in this work are added in Table S.I.4. It is clear that the adsorption capacity of MPC-1 is superior to coconut shell-based commercial activated carbon (CS-AC), ML and some other previously reported

adsorbents.[4,19,21,40,41,42]

3.4. Adsorption kinetics.

The kinetics of adsorption is important because this is what controls the efficiency of the process and the time to reach equilibrium. It also describes the rate of adsorbate uptake on nanoporous carbons. In order to identify the potential rate controlling steps involved in the process of adsorption, three kinetic models were studied and used to fit the experimental data from the adsorption of dyes onto nanoporous carbons. These models are the pseudo-first-order,[43] pseudo-second-order[44] and intra-particle diffusion models.[45] These models can be expressed as:

Pseudo-first order model: $\ln(q_e - q_t) = \ln(q_e) - K_1 t$ (10)

Pseudo-second order model: $\frac{t}{q_t} = \frac{1}{K_2 q_e} + \frac{t}{q_e}$ (11)

Intra-particle diffusion model: $q_t = K_3 t^{1/2}$ (12)

where q_e and q_t (mg/g) are the uptake of OII and ACBK at equilibrium and at time t (min), respectively, K_1 (1/min) is the adsorption rate constant, K_2 (g/mg min) is the rate constant of second-order equation, K_3 (mg/g $\text{min}^{1/2}$) is the intra-particle diffusion rate constant.

In order to quantitatively compare the applicability of different kinetic models in fitting to data, a normalized standard deviation, $\triangle q$ (%), was calculated as below:

$$\Delta q(\%) = \frac{(q_{e,\exp} - q_{e,cal})}{q_{e,\exp}} \times 100\% \quad (13)$$

The effect of contact time on adsorption capacities of MCP-1 to OII and MO from single and binary dye solutions are shown in Fig. 7. These figures show that the

adsorption capacities for OII and MO increase with the increase of contact time, and the adsorption reaches equilibrium within about 1 h. The saturation capacities of OII and MO onto MCP-1 in the single dye solution are 1488 and 869 mg/g at room temperature (298 K), 3 h contact time, 1000 mg/L initial concentration, 7 pH value and 0.4 g/L adsorbent dose. For single and binary dye adsorption systems, the adsorption capacities of OII and MO were reduced from 1488 mg/g (single system) to 869 mg/g (binary system) and from 869 mg/g (single system) to 447 mg/g (binary system), respectively, at pH 7 because of the highly contention on active sites between two types of dye molecules in the binary system. The capacity is constant when all the parametrs are fixed, and with the evolution of time, the uptake or adsorbed amount may change. The fast adsorption at the initial stage may be due to the availability of the uncovered surface area and the remaining active sites on the adsorbent.

The experimental kinetic data of OII and MO, calculated from Eqs. (10), (11) and (12), were correlated by three kinetic models: pseudo-first order, pseudo-second order and intra-particle diffusion models. The calculated constants of the three kinetic equations along with R^2 values at different temperatures are presented in Table S.I.5. As seen in Table S.I.5, there is a large difference between the experimental and calculated adsorption capacity values when the pseudo-first order was applied. However, high R^2 values (>0.999) are obtained with the linear plot of t/q_t versus t, suggesting the pseudo-second order adsorption kinetics. Additionally, the pseudo-second order kinetic model kinetic model is in a good agreement with the experimental and calculated adsorption capacity values Δq (%). If the intra-particle

diffusion is the mechanism of the adsorption process, then the plot of q_t versus $t^{1/2}$ will be linear and if the plot passes through the origin, then the rate limiting process is only due to the intra-particle diffusion. Otherwise, some other mechanism along with intra-particle diffusion is also involved.[33] However, as shown in Fig. 8, the plots are not linear over the whole time range and, instead, can be separated into multi-linear curves, illustrating that multiple stages were involved in the adsorption process. The first straight portion was attributed to the macro-pore diffusion (phase I) and the second linear portion was attributed to micro-pore diffusion (phase II). The results indicated that the adsorption of OII and MO dyes onto MCP-1 involved more than one process, and the intra-particle transport is not the rate-limiting step. Such finding is similar to that made in previous works.[3,19,35]

3.5. Desorption process

Generally, there are two techniques for desorption of the adsorbent: the thermal treatment and the solvent elution.[46,47] Based on the solvent elution procedures of the literatures,[46-48] the reservation of the dyes on the MPC-1 is about 80 % after washing with organic solvent, acid or alkali media. The results demonstrated that the MPC-1 has a relative good absorption ability for the anionic dyes (OII and MO). In addition, although nearly 90 % of the MPC-1 saturated by the dyes can be regenerated after thermal treatment at a stream of nitrogen at 973 K, we not attempted to cyclically utilize the porous carbon due to its low cost in preparation.

4. Conclusion

The present study shows that the MPC-1 from biomass waste is an effective

adsorbent for the removal of OII and MO from single and binary dye aqueous solution. Adsorption ability of the Batch adsorption tests demonstrate that the adsorption is affected by various conditions such as contact time, solution pH and initial dye concentration. The equilibrium data of the removal strongly follow the Langmuir monolayer adsorption with high adsorption capacity in a short amount of time. The kinetics studies showed applicability of pseudo-second-order model. Weber and Morris plot verified the adsorption mechanism was due to multi-linearity correlation. The π-π stacking interaction between the surface of porous carbon and dyes could be one of the important responsiblity for the high adsorptive performance of the MPC-1. Therefore, we conclude that MPCs material can be used as highly efficient adsorbents and reused for the removal of anionic azo-dyes from wastewater.

Corresponding Author

*[a] E-mail: daiwei@zjun.edu.cn. Fax: +86-579-82282531. Tel:+86-579-82282269.

*[b] E-mail: mana@zjun.cn. Fax: +86-579-82283595. Tel:+86-579-82283595.

Acknowledgments

This work was supported by the Public Projects of Zhejiang Province of China (No. 2015C31083) and Zhejiang Qianjiang Talent Project (No. QJD1302014).

Notes and references

1 J. Li, D. Ng, P. Song, C. Kong, Y. Song and P. Yang, *Biomass Bioenerg*., 2015, **75**, 189.

2 W. Dai, H. Yu, N. Ma and X Yan, *Korean J. Chem. Eng.*, 2015, **32**, 335.

3 L. Shao, Y. Yao, S. Quan, H. Wei, R. Wang and Z. Guo, Mater. Lett., 2014, **114**, 111.

4 C. Hsiu-Mei, C. Ting-Chien, P. San-De and C. Hung-Lung, *J. Hazard. Mater*. 2009, **161**, 1384.

5 J. S. An, Y. J. Back, K. C. Kim, R. Cha, T. Y. Jeong and H. K. Chung, *Environ. Technol*. 2014, **35**, 1668.

6 C. R. Li, Z. Y. Zhuang, F. Huang, Z. C. Wu, Y. P. Hong and Z. Lin, *ACS Appl. Mater. Interfaces*, 2013, **5**, 9719.

7 X. Du, H. Zhang, X. Hao, G. Guan and A. Abudula, *ACS Appl. Mater. Interfaces* 2014, **6**, 9543.

8 L. Fu, C. Shuang, F. Liu, A. Li, Y. Li, Y. Zhou and H. Song, *J. Hazard. Mater.* 2014, **272**, 102.

9 Y. K. Ong, F. Y. Li, S. P. Sun, B. W. Zhao, C. Z. Liang and T. S. Chung, Chem. Eng. Sci., 2014, **114**, 51.

10 L. Shao, X. Q. Cheng, Y. Liu, S. Quan, J. Ma, S. Z. Zhao and K. Y. Wang, *J. Membrane Sci.*, 2013, **430**, 96.

11 S. J. Deng, R. Wang, H. J. Xu, X. S. Jiang and J. Yin, *J. Mater. Chem.* 2012, **22**, 10055.

12 S. J. Deng, H. J. Xu, X. S. Jiang and J. Yin, *Macromolecules*, 2013, **46**, 2399.

13 B. Li, Y. C. Dong, C. Zou and Y. M. Xu, *Ind. Eng. Chem. Res*., 2014, **53**, 4199.

14 A. Yadav, S. Mukherji and A. Garg, *Ind. Eng. Chem. Res*., 2013, **52**, 10063.

15 C. S. D. Rodrigues, L. M. Madeira and R. A. Boaventura, *Ind. Eng. Chem. Res.*, 2014, **53**, 2412.

16 B. E. Tastan, S. E. Karatay and G. Donmez, *Water Sci. Technol.*, 2012, **66**, 2177.

17 J. Hu, H. J. Yu, W. Dai, X.Y. Yan, X. Hu and H. Huang, *RSC Adv.*, 2014, **4**, 35124.

18 F. Liu, S. Chung, G. Oh and T. S. Seo, *ACS Appl. Mater. Interfaces*, 2012, **4**, 922.

19 R. Gong, J.Ye, W. Dai, X. Yan, J. Hu, X. Hu, S. Li and H. Huang. *Ind. Eng. Chem. Res.*, 2013, **52**, 14297.

20 Md. Islam Azharul, I. A. W. Tan, A. Benhouria, M. Asif and B. H. Hameed, *Chem. Eng. J.*, 2015, **270**, 187.

21 F. Güzel, H. Saygli, G. A. Saygli, F. Koyuncu, *J. Mol. Liq.*, 2014, **194**, 130.

22 T. E. Rufford, D. Hulicova-Jurcakova, K. Khosla, Z. H. Zhu and G. Q. Lu, *J. Power Sources*, 2010, **195**, 912.

23 C. Peng, X. B. Yan, R. T. Wang, J. W. Lang, Y. J. Ou and Q. J. Xue, *Electrochim. Acta.*, 2013, **87**, 401.

24 X. L. Wu, T. Wen, H. L. Guo, S. B. Yang, X. K. Wang and A. W. Xu, ACS *Nano.*, 2013, **7**, 3589.

25 Y. K. Lv, L. H. Gan, M. X. Liu, W. Xiong, Z. J. Xu,; D. Z. Zhu and D. S. Wright, *J. Power Sources*, 2012, **209**, 152.

26 D. Jimenez-Cordero, F. Heras, M. A. Gilarranz and E. Raymundo-Pinero, *Carbon*, 2014, **71**, 127.

27 X. Li, W. Xing, S. P. Zhuo, J. Zhou, F. Li, S. Z. Qiao and G. Q. Lu, *Bioresource Technol*., 2011, **102**, 1118.

28 S. H. Du, L. Q. Wang, X. T. Fu, M. M. Chen, C. Y. Wang, *Bioresource Technol*., 2013, **139**, 406.

29 X. J. He, R. C. Li, J. S. Qiu, K. Xie, P. H. Ling, M. X. Yu, X. Y. Zhang and M. D. Zheng, *Carbon*, 2012, **50**, 4911.

30 Q. Wang, J. Yan, Y. B. Wang, T. Wei, M. L. Zhang, X. Y. Jing and Z. J. Fan, *Carbon*, 2014, **67**, 119.

31 T. Katekunlaphan, R. Chalermglin, T. Rukachaisirikul, P. Chalermglin, *Biochem. Syst. Ecol*., 2015, **57**,152.

32 M. L. Yola, T. Eren, N. Atar and S. Wangc, *Chem. Eng. J*., 2014, **242**, 333.

33 L. Shao, Z. X. W. Y. L. Zhang, Z. X. Jiang and Y. Y. Liu, J. Membrane Sci., 2014, **461**, 10.

34 A. Barroso-Bogeat, M. Alexandre-Franco, C. Fernández-González and V. Gómez-Serrano, *Energy Fuels*, 2014, **28**, 4096.

35 Á. S ánchez-S ánchez, F. Su árez-Garc á, A. Mart ínez-Alonso and J. M. D. Tasc ón, *J. Colloid Interf. Sci.*, 2015, **450**, 91.

36 I. Langmuir, *J. Am. Chem. Soc*., 1918, **40**, 1361.

37 H. Freundlich, *J. Phys. Chem*., 1906, **57**, 385.

38 M. I. Temkin and V. Pyzhev, *Acta Physiochim. URSS*., 1940, **12**, 327.

39 M. M. Dubinin and L. V. Radushkevich, *Dokl. Akad. Nauk. SSSR*., 1947, **55**, 327.

40 R. S. Ribeiro, N.A. Fathy, A. A. Attia, A. M. T. Silva, J. L. Faria and H. T. Gomes, *Chem. Eng. J*., 2012, **195**, 112.

41 M. Ghaedi, F. Mohammdi and A. Ansari, *J. Disper. Sci. Technol*., 2015, **36**, 652.

42 M. Ahmaruzzaman and R. A. Reza, *Environ. Prog. Sustain*., 2014, **34**,724.

43 S. Langergen, B. K. Svenska, *Veteruskapsakad Handlingar*, 1898, **24**, 1.

44 Y. S. Ho and G. Mckay, *Process Biochem*., 1999, **34**, 451.

45 G. Annadurai, R. S. Juang and D. J. Lee, *J. Hazard. Mater*., 2002, **92**, 263.

46 H. I. Chieng, N. Priyanthabc and L. B. L. Lim, *RSC Adv*., 2015, **5**, 34603.

47 M. R. Malekbala, M. A. Khan, S. Hosseinia, L.C. Abdullah and T. S.Y. Choonga, *J. Ind. Eng. Chem*., 2015, **21**, 369.

48 L. Liu, Z. Y. Gao, X. P. Su, X. Chen, L. Jiang, and J. M. Yao, *ACS Sustainable Chem. Eng.* 2015, **3**, 432−442.

Scheme 1. Chemical structures of OII (A) and MO (B).

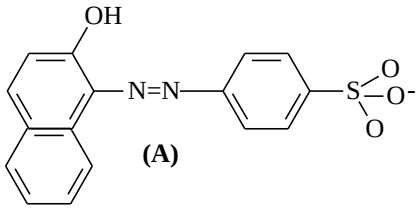

(A)

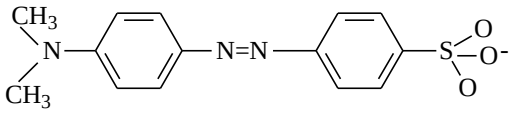

(B)

Figure captions:

Fig. 1 Nitrogen adsorption isotherm and pore size distribution.

Fig. 2 TEM and SEM images of the prepared MPC-1 (A) and ML (B)

Fig. 3 FTIR spectrums of ML and MPC-1

Fig. 4 Effect of MPC-1 dose on adsorption of OII and MO in SDS and BDS systems.

Fig. 5 Effect of pH on adsorption of OII and MO in BDS and SDS.

Fig. 6 Adsorption isotherms of OII and MO on MPC-1 in SDS and BDS, respectively.

Fig. 7 Effect of contact time on the adsorption capacities of OII and MO on MPC-1 in SDS and BDS systems.

Fig. 8 Weber–Morris intra-particle diffusion plots for the adsorption of OII and MO on MCP-1 in SDS and BDS.

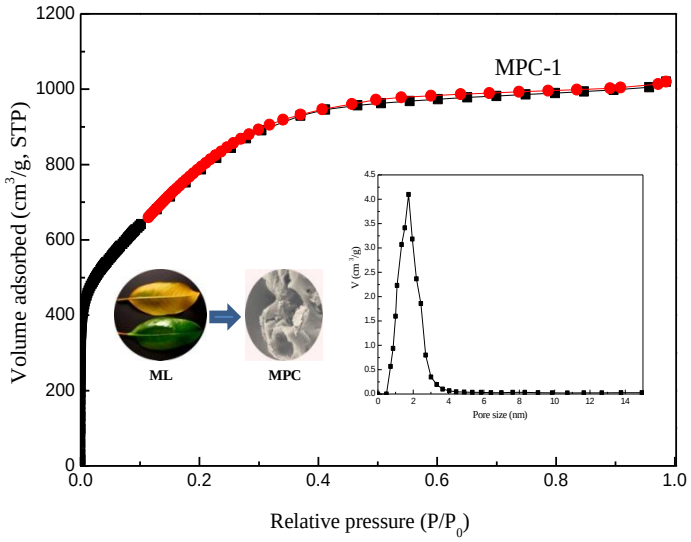

Fig. 1 Nitrogen adsorption isotherms and pore size distributions

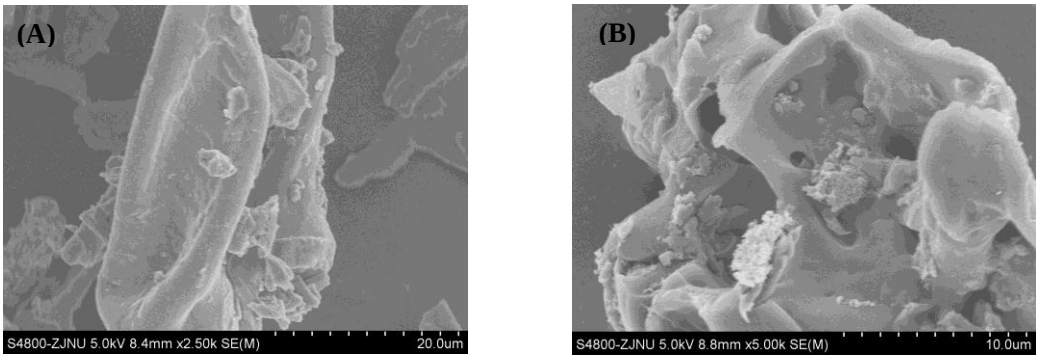

Fig. 2 TEM and SEM images of the prepared ML (A) and MPC-1 (B)

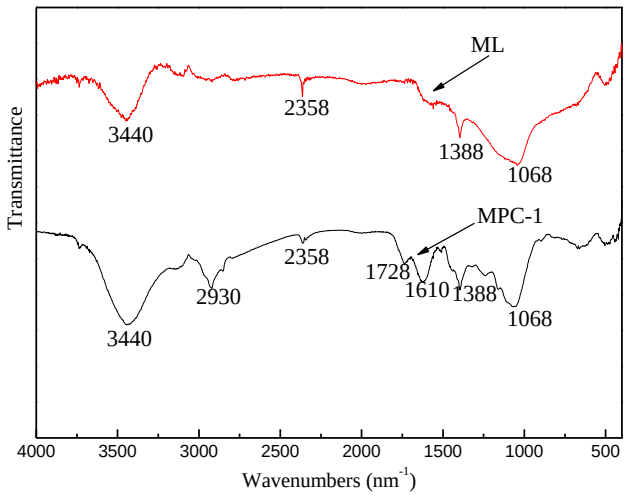

Fig. 3 FTIR spectrums of ML and MPC-1

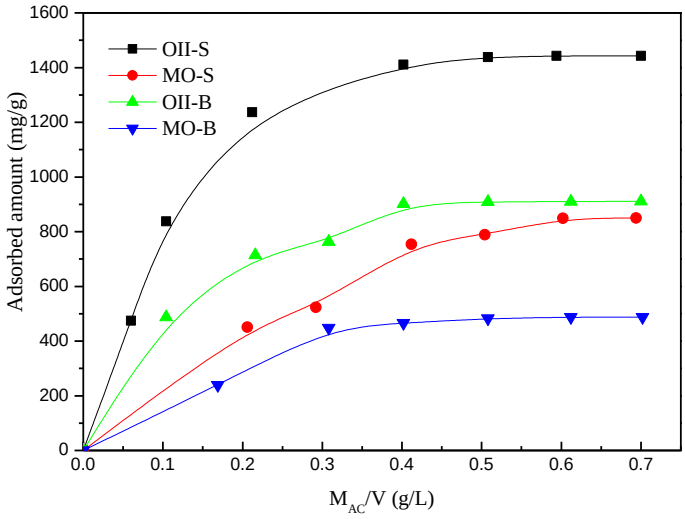

Fig. 4 Effect of MPC-1 dose on adsorption of OII and MO in SDS and BDS systems.

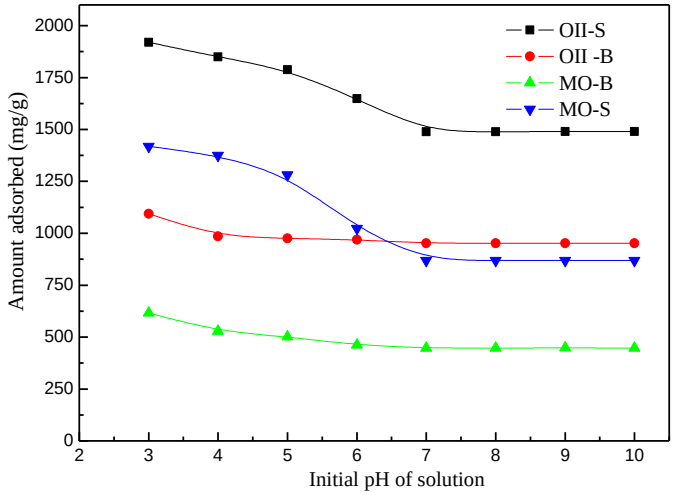

Fig. 5 Effect of pH on adsorption of OII and MO in BDS and SDS.

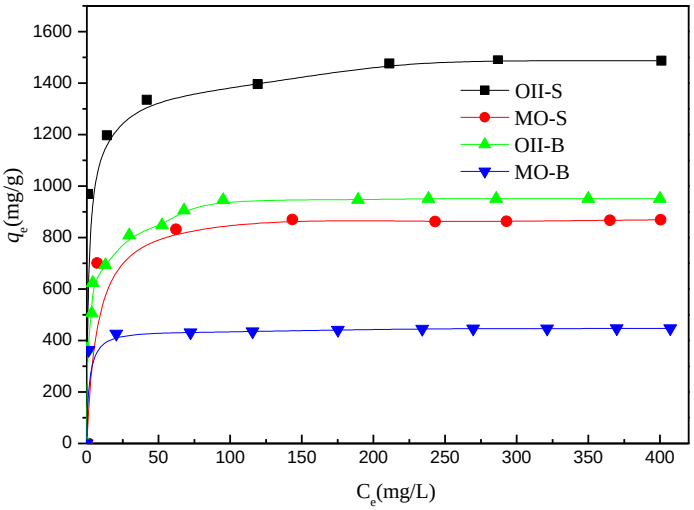

Fig. 6 Adsorption isotherms of OII and MO on MPC-1 in SDS and BDS, respectively.

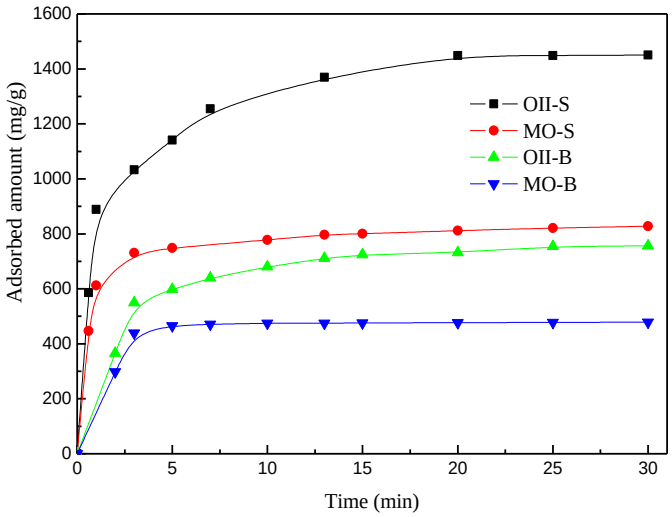

Fig. 7 Effect of contact time on the adsorption capacities of OII and MO on MPC-1 in SDS and BDS, respectively.

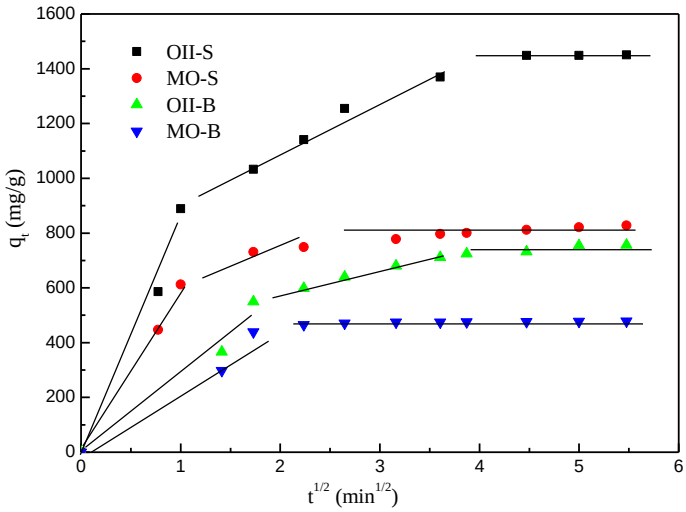

Fig. 8 Weber–Morris intra-particle diffusion plots for the adsorption of OII and MO on MCP-1 in SDS and BDS, respectively.